



Contents lists available at ScienceDirect

Sensors and Actuators B: Chemical

journal homepage: www.elsevier.com/locate/snb

Enhancing the sensitivity of point-of-use electrochemical microfluidic sensors by ion concentration polarisation – A case study on arsenic

Vidhya Subramanian^{a,b}, Sangjun Lee^c, Sanjoy Jena^d, Sourav Kanti Jana^a, Debdutta Ray^d, Sung Jae Kim^{c,e,f}, Pradeep Thalappil^{a,*}

^a DST Unit on Nanoscience and Thematic Unit of Excellence (TUE), Department of Chemistry, Indian Institute of Technology, Madras, Chennai 600 036, India

^b Department of Biotechnology, Indian Institute of Technology, Madras, Chennai 600 036, India

^c Department of Electrical and Computer Engineering, Seoul National University, Seoul 08826, Republic of Korea

^d Department of Electrical Engineering, Indian Institute of Technology, Madras, Chennai 600 036, India

^e Inter-University Semiconductor Research Center, Seoul National University, Seoul, South Korea

^f Nano Systems Institute, Seoul National University, Seoul, South Korea

ARTICLE INFO

Keywords:

Point of use sensor
Electrochemical microfluidic sensor
Ion concentration polarisation
Arsenic
Heavy metal ions

ABSTRACT

Point of use (POU) sensors are extremely relevant, being capable of providing fast and reliable analysis in remote and resource-limited settings. Of all the diverse techniques utilised for POU sensors, a combination of electrochemistry and microfluidics may have the greatest potential towards quantitative assessment of heavy metal ions. The major challenge in combining these for sensing applications lies in the complexity of fabricating integrated devices and the insufficient quantity of analytes in the sample volume. To address these issues, we have developed a radial microfluidic device capable of electrokinetic preconcentration by ion concentration polarization (ICP) and integrated it with electroactive surfaces. The proposed sensor is the first demonstration of concentration of heavy metal ions by ICP and its quantitative assessment by voltammetry. Utilising the integrated sensor, we have shown the sensing of As^{3+} down to 1 ppb by linear sweep voltammetry with $\sim 40 \mu\text{L}$ of sample. The sensor was also tested successfully for sensing As^{3+} in a field sample from an arsenic affected region of India. The sensor was also tested for the detection of other metal ions too. This work would facilitate the development of highly sensitive POU hand-held sensors for water quality monitoring in resource-limited areas.

1. Introduction

Presence of naturally occurring arsenic in water is of particular concern and has received considerable attention owing to its high toxicity. Specifically, trivalent form of arsenic (As^{3+}) has been noted to cause various adverse health effects ranging from vomiting, abdominal pain, etc., in case of acute poisoning while chronic exposure can lead to skin, lungs and bladder cancer [1]. Arsenic compromises the body's immune functions, damages lung cells and causes inflammation of heart cells. Presence of 19 ppb of arsenic in human body reduces lung functions considerably and when it is above 120 ppb, the lung's ability is affected to the same extent as that of long term smokers [2]. Being tasteless and odorless in water, the presence of arsenic cannot be detected easily. For accurate detection of arsenic, various lab - based instrumentation [3] such as atomic absorption spectroscopy (AAS) [4] and inductively coupled plasma mass spectrometry (ICP-MS) [5] exist. Though these instruments provide accurate measurements, their

shortcoming lies in their size and requirement of trained personnel which limit their portability. One of the techniques that can be used to address these issues is electrochemistry [2]. Electrochemical sensors are based on the transfer of electrons on the surface of the electrodes and their advantages lie in low cost with ease of miniaturization, minimal sample pre-treatment and portability [6]. The advantage of portability in utilising electrochemical sensors arise from the fabrication and development of portable potentiostats that can perform most of the electrochemical measurements. Portable electrochemical detectors are currently being extensively researched upon because of their potential value in point-of-use applications [7–9]. Added advantage of such a system lies in its use as peripheral devices which can be integrated with mobile phones through bluetooth and the data can be uploaded to a data storage system anywhere in the world using the current mobile technology making it useful in resource limited settings [8] for remote monitoring of remediation solutions. These parameters of the electrochemical sensors make it suitable for developing point of use sensors for

* Corresponding author.

E-mail address: pradeep@iitm.ac.in (P. Thalappil).

<https://doi.org/10.1016/j.snb.2019.127340>

Received 17 September 2019; Received in revised form 23 October 2019; Accepted 24 October 2019

0925-4005/© 2019 Elsevier B.V. All rights reserved.

arsenic and other metallic elements [10].

Integrating electrochemistry to microfluidics has given rise to the development of electrochemical microfluidic devices leading to micro total analysis systems (μ TAS). The advent of μ TAS changed the outlook for various applications [11,12]. Microfluidics form the core technology in μ TAS owing to its versatility and requirement of smaller volumes for analysis. The major constraint one encounters while using microfluidics for sensors is the insufficient amount of analytes in the volume utilised. To rectify this, various preconcentration techniques such as isoelectric focusing [13], electric field gradient focusing [14], electrokinetic trapping [15], immunocapture based trapping [16], etc. [17], are being looked at. Of particular interest is electrokinetic trapping where in the presence of micro-nano junctions in a microchannel, different phenomena like ion exclusion enrichment effect, ion depletion enrichment effect, and amplified electrokinetic effect are exhibited [18,19] near the micro-nano interface. During electrokinetic trapping, the application of an external electric field results in an ion imbalance between the microchannel and nanochannel due to electro-migration flux, inducing the formation of a concentration gradient near the micro/nanochannel interface. This causes a diffusion flux which works to balance the ion flux of the system. The micro-nano junction is usually created by placing a membrane in the microchannel, where the nanopores of the membrane in contact with the microchannel form the micro-nano junction. These membranes are preferably electronegative with preferential cation permeability, where the charge selectivity is caused by the acidic impurities present on the pores of the membrane [20]. This technique has been termed as ion concentration polarization (ICP). Although the abbreviation ICP is commonly used for inductively coupled plasma, we propose to use the same as the literature has accepted it. ICP has been extensively used for the concentration of dyes, biomolecules, etc. [21–23]. Multiple theoretical studies have been performed to understand the mechanism of concentration and the scaling laws involved [24].

Here in this paper, we have integrated a radial channel ICP device directly to electrodes to perform electrochemistry. Even though ICP is capable of concentrating ions in microchannel, its major limitation lies in the incapability to quantitatively analyse the concentrated analyte, hence limiting most of the ICP devices to qualitative analysis. We have rectified this issue by combining our microfluidic devices to electrodes. Radial microchannels were utilized to increase the analyte volume used for preconcentration. The device design was kept simple to enable ease of fabrication and analysis. Multiple ions were analysed in the device to study their concentration mechanism and detection by voltammetry, with particular interest to arsenic.

2. Experimental

2.1. Materials

Gold wire, chrome pellets, silver wire, platinum wire, copper (II) acetate, lead (II) acetate, iron (II) acetate and manganese (II) acetate were purchased from Sigma – Aldrich. Sodium arsenite was purchased from SD Fine Chem Ltd. Potassium hydroxide, sulphuric acid (H_2SO_4), acetone and iso-propyl alcohol were sourced from Rankem. Sylgard kit was purchased from Dow-Corning. Nafion perfluorinated resin solution was purchased from Aldrich. All chemicals were of analytical grade and were used without further purification. Distilled water was used throughout the experiments unless mentioned otherwise.

2.2. Instrumentation

For the electrode fabrication, spin coating was performed using Spin Coaters Spin 150 followed by UV beam exposure in mask aligner using OAI model 5000. For chrome and gold deposition, electron beam lithography was performed using BOC Edwards Auto 306. Scanning electron microscope (SEM) images were taken using FEI QUANTA-200

SEM. Spin coating of PDMS was performed using Spin NXG – P1a. Plasma bonding was done using Harrick Plasma Plasma Cleaner PDC-002-HP. The electrochemical measurements were performed using CHI 600A (CH Instruments, USA). External voltage was applied using Keithley 2611 B sourcemeter. Optical Imaging was done using Leica DMI 3000 B inverted microscope.

2.3. Electrode fabrication

The gold electrodes on glass were patterned using photolithography. The process included the heating of glass slides in an oven at 120 °C followed by spin coating of SU-8 photoresist on the substrate and further baking at 60 °C. The photoresist coated slide was then exposed to UV beam for 20 s through the mask. The exposed substrate was developed by placing in KOH solution for 20 s. The patterned slide was then washed in distilled water and blow dried. Gold was deposited on these substrates by electron beam deposition and subsequently washed in IPA to remove the excess followed by washing in distilled water and blow dried by N_2 gas. Thickness of the electrode was maintained at 80 nm with 5 nm chrome layer and 75 nm gold layer. The fabrication process is demonstrated in SI Figure S1.

2.4. Microchannel fabrication

We designed an 8-way radial channels with 100 μm height, 100 μm width and 1 cm length. The master wafer was fabricated using standard photolithography process [25]. The radial devices were then fabricated by using standard soft lithography technology from literature [26]. The inlet and outlet for the channels were made using a 2 mm punch.

2.5. Patterning of perm-selective membrane

We patterned a circular nafion film on a 250 μm thick PDMS layer with a 2 mm central hole by stamping method. The radius of the stamp was 2.5 mm. The PDMS film was then heated on a hotplate at 75 °C for 5 min to remove the solvent.

2.6. Chip fabrication

The fabricated device was composed of four layers: radial microchannels (top layer), nafion patterned PDMS layer with 2 mm hole (second layer from top), PDMS layer with 3 mm hole interconnecting the sensing layer and the concentration layer (third layer from top) and electrochemical sensor (bottom layer). Two layers from the top acted as the working layer. Nafion in the second layer was patterned in a circular manner of diameter 2.5 mm to enable the concentration in all the 8 microchannels. This design caused the ions to concentrate at the centre of the 8 channels. The 2 mm hole at the centre of the second layer acted as the pathway for the concentrated ions to move towards the electrodes. The diameter of the hole was optimised at 2 mm to minimise the trapping of bubbles in the bottom two layers. The third layer was composed of a PDMS layer with a 3 mm window. The thickness for the second and third layer were maintained as 250 μm each. The bottom layer consisted of 3 electrodes patterned in a circular manner with a total diameter of 2.5 mm.

2.7. Electrochemical measurements and data analysis

The electrochemical measurements were performed by an electrochemical workstation at room temperature. Electrochemical measurements were carried out using a three electrode system consisting of bare gold as working and counter electrodes. Silver wire was used as the reference electrode. To monitor the stability of the electrodes, the device was continuously observed using an inverted microscope during the experiment.

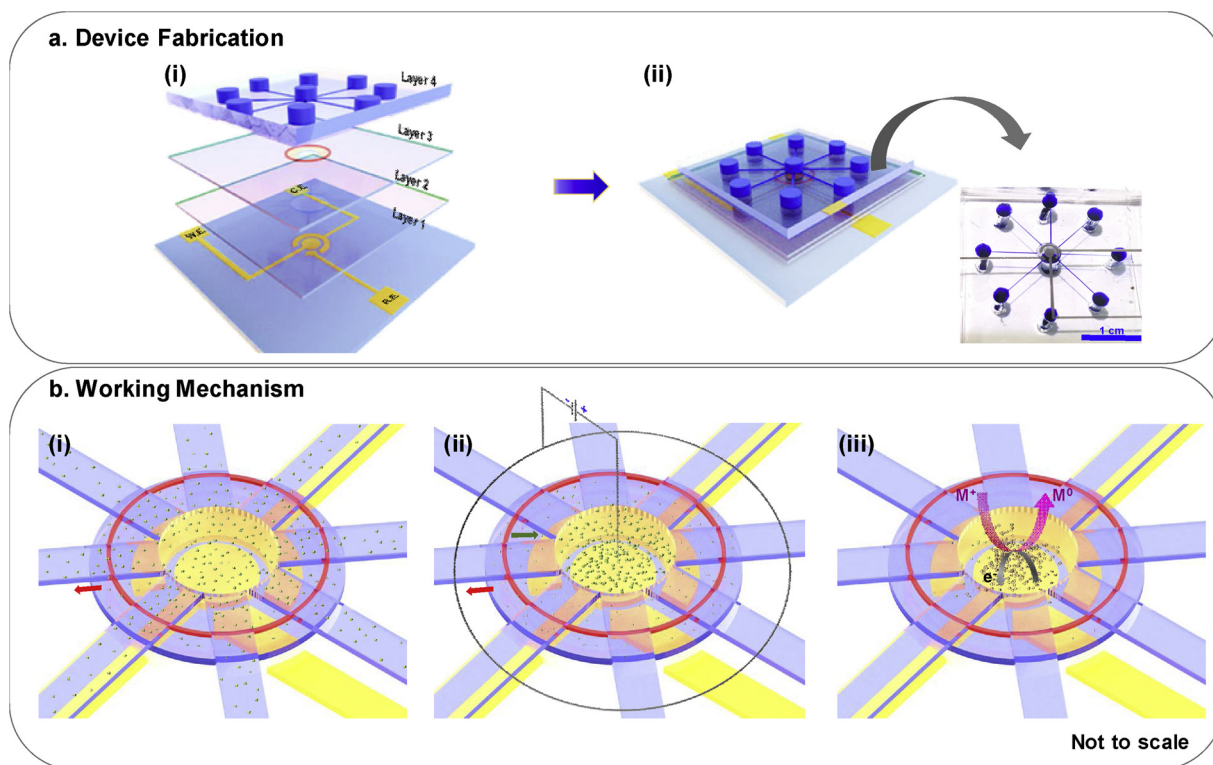


Fig. 1. A schematic of the device fabrication protocol and its working mechanism. Panel a shows the device fabrication, (i) representation of the various layers of the device, Layer 1 contains the electrodes, Layer 2 consists of a 3 mm window at the center, Layer 3 contains a 2 mm window at the center along with circularly patterned nafion of 2.5 mm radius and Layer 4 contains the microchannels, (ii) shows the fully fabricated device, inset shows an optical image of the fabricated device (bottom view). Panel b shows the working mechanism of the device. (i) schematic showing the top view of the device, the device is filled with the analyte, outward (red) arrow depicts the direction of flow (ii) represents application of external voltage (anode is placed at the central well and ring electrode at the outer wells) to induce ion concentration, inward (green) arrow shows the direction of ion movement and (iii) upward (magenta) arrow at the center of the radial device depicts the reduction of concentrated ions after ICP.

3. Results and discussion

3.1. Characterization of the electrodes and microfluidic device

The optical image of the electrode is given in the inset of SI Figure S2a. The surface morphology of the electrodes was analysed using SEM as represented in SI Figure S2a. SEM images showed that the electrodes have a homogeneous surface. The dimensions of the electrode are given in SI Figure S2b. For the electrochemical characterization of the fabricated electrodes, cyclic voltammetry (CV) of ferro/ferricyanide complex was performed, given in SI Figure S3. We observed reversible redox peaks at the electrolyte - electrode interface confirming that the electrode surface was electroactive. Ion concentration polarization in a radial microfluidic device has already been established [27,28].

3.2. Working mechanism

The experimental steps involved in the fabrication and sensing is depicted in Fig. 1. After fabricating the device, the sample is injected by utilising a commercial pipette tip. The pipette tip was placed at the centre of the radial device and the sample was injected into the microchannels by applying pressure. Volume of the sample present in the microchannels at any given time during the analysis was calculated to be 8 μL while the total volume in the device was $\sim 40 \mu\text{L}$. Detailed calculations for analyte volume in the microchannels and the device are given in SI S4. Following this, the measurements were carried out in two steps. The first step involved the application of an external DC voltage to the platinum wire placed in the micropipette tip containing the analyte to induce ICP. This voltage is applied for a stipulated time to induce ion concentration. The next step was to do the voltammetry

measurements. These measurements were initiated 3 s after the externally applied voltage is switched off. The intermediate 3 s acted as the buffer time to minimise the noise due to external applied voltage on the working electrode.

3.3. Working principle

ICP is an electrokinetic phenomenon consisting of dynamic ion concentration changes with ion depletion and ion enrichment across nanochannels/nanopores [19]. Cation exchange membranes such as nafion use sulfone anion (R-SO_3^-) as a fixed charge making it cation selective by nature [20]. When an analyte is flowed in a microchannel connected to a cation selective membrane and a DC electric field is applied, only cations will pass through the micro-nano junction while anions will concentrate on the other side of the membrane. To satisfy the laws of electro-neutrality, an extended space charge (ESC) layer forms adjacent to the electrical double layer [28,29]. By varying the applied voltage, both anions and cations can be pushed towards the anode leading to an ion enriched zone at the cathodic side of the nanochannel and ion depletion zone on the other side [30]. In contrast to the conventional ICP devices, which utilise a buffer channel along with the analyte channel, our devices work on the concept of “a bufferchannel-less radially structured preconcentrator” [28]. The use of a radial configuration enhances throughput, electrokinetic stability and causes local increase in concentration at the centre of the device during ICP. In our device, the anode was placed perpendicular to the electrodes meant for voltammetry. After the ions were concentrated at the anode by ICP, the concentration of the ions was analysed by linear sweep voltammetry.

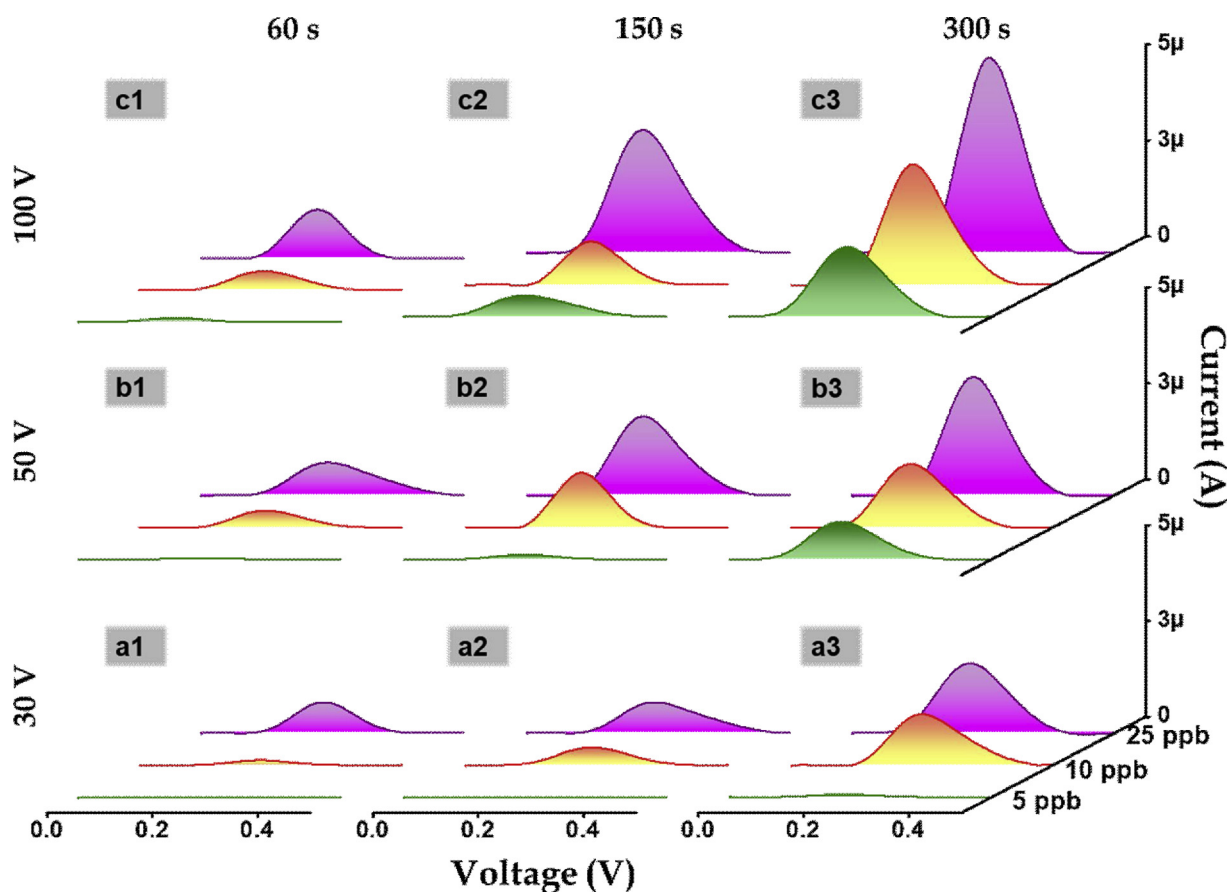


Fig. 2. Electrochemical characterization of As^{3+} after ICP. The x-axis represents the voltage applied during voltammetry and the current is plotted in y-axis. Green trace represents 5 ppb of As^{3+} in 0.1 M H_2SO_4 , while orange and magenta traces are for 10 and 25 ppb, respectively. Voltage applied during ICP is given as a, b and c which stand for 30, 50 and 100 V respectively. Labels 1, 2 and 3 depict the durations for which the voltages were applied, which were 60, 150 and 300 s respectively. For example, a1 represents LSV obtained after applying 30 V for 60 s during ICP.

3.4. Ion pre-concentration and detection

The fabricated chip was utilised to concentrate the ions in the sample. To study the concentration effects with varying time and voltage, the pre-concentration was carried out by applying 30, 50 and 100 V in varying durations of 60, 150 and 300 s for 5, 10 and 25 ppb of As^{3+} in 0.1 M H_2SO_4 . After concentrating, linear sweep voltammetry was utilised for quantitative assessment of analyte concentration. For linear sweep voltammetry, potential for the measurements were optimised from 0 to 5 V, since the oxidation peak of As^{3+} in acidic medium is known to be at 0.21 V.

Fig. 2 shows the voltammogram of the concentrated ions. For clearer understanding, the values are tabulated in SI Table 1. It is known that at acidic pH, As^{3+} exists as H_3AsO_3 which is neutral in charge [31].

The experiment was expected to proceed in two steps, the first step involved a local increase in the concentration of ions in the vicinity of the working electrode caused by ICP. This was followed by the oxidation and reduction of metal ions on the working electrode during LSV as given in eqn. 1 and eqn. 2.

As such, it was expected that the combination of ICP with LSV acts similar to Anodic Stripping Voltammetry (ASV). In ASV, the first step is to apply a controlled potential to deposit the metal ions on the working electrode. This causes the local increase in concentration of analyte by depositing the ions from the larger volume of solution to the electrode. This is then followed by stripping of the electrode for measurements. Major limitation in ASV arises due to the incomplete stripping of the working electrode after deposition, effectively reducing the surface active sites available in the electrode for subsequent measurements

[32]. This limitation was rectified in our device, as during ICP the local increase in concentration of the ions is caused by transferring the ions from the microchannels to the 3 mm well where the electrodes are located without affecting the working electrode during the concentration process and reducing the ion residence time on the electrodes. This results in no or reduced effect on the active sites of the working electrode. For our experiments, the peak value of As^{3+} was noted to be 0.21 ± 0.02 V. The shift can be attributed to the deviation in ionic current of the electrolyte as a result of applying potential to the microchannels during ICP. The buffer time between the application of ICP voltage and voltammetry measurements was optimised to 3 s. If the buffer time is lesser, the background current is too high, resulting in increase in noise in the voltammogram. In case its more than 3 s, there is a loss in the ions concentrated by ICP.

There was no peak seen in the absence of ICP. The minimum current obtained for 5 ppb at 30 V was 3.49×10^{-3} μA after concentrating for 60 s. No voltammetric peaks were seen at reduced potential or time. From this it can be understood that 30 V was the voltage required for a stable junction formation at the micro-nano interface. Upper threshold voltage was determined by doing ICP at 100 V up to which we obtained linear increase in voltammetric current. ICP performed with applied voltage of 150 V did not show linearity in concentration which is due to the instability of the junction. Maximum current for 5 ppb was observed during the application of 100 V for 300 s and it was 1.82 μA while the application of 30 V to a 5 ppb solution for the same duration exhibited a current of 6.02×10^{-2} μA showing a 30-fold increase in the current intensity. Measurements for the concentration of 10 ppb and 25 ppb when concentrated for 300 s, at 30 and 100 V, showed a 3-fold enhancement in the current. Except for the minimum concentration of

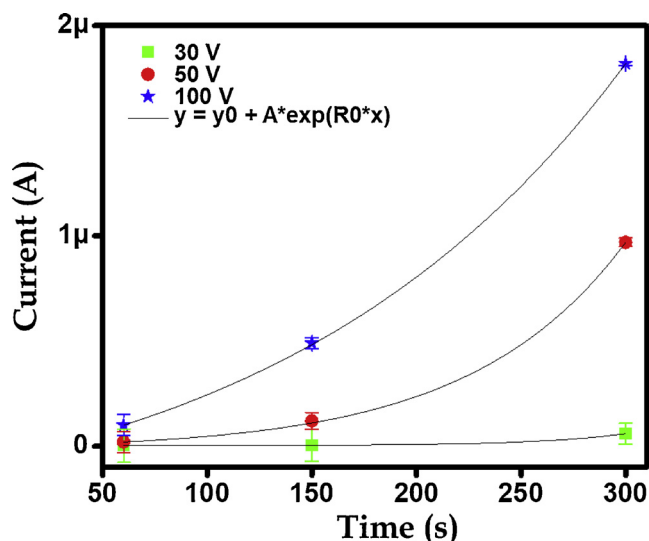


Fig. 3. Variation of the voltammetric signal at the peak voltage (0.21 V) for 5 ppb As^{3+} with time at different ICP voltages. The data are fitted with straight lines.

5 ppb, ICP of 10 and 25 ppb showed similar concentration enhancement factors. Applying voltage for a longer time will result in higher concentration of ions at the anode. The maximum time for ICP was kept at 300 s taking into account its possible use as a point of use sensor where shorter analysis time is a major requirement. WHO's provisional guideline for arsenic in drinking water is 0.01 mg/l i.e. 10 ppb, hence, all the experiments were conducted with 5 ppb as lower limit.

From the literature [22,33], it is known that ICP is an ion transport phenomenon caused by the selective passage of ions through ion exchange membranes. Nafion being a cation permeable membrane allows the selective passage of cations restricting the movement of anions. In the presence of an external voltage, the anions are attracted to the anode while to maintain electroneutrality, the cations also move to the anodic side. This leads to the increase in the concentration of ions at the anode which in turn results in the increase in the local ion concentration around the electrodes meant for voltammetry as these electrodes are placed directly below the anode. This results in the better detection, although the samples have lower bulk concentration. Fig. 3 shows the voltammetric signal of As^{3+} at the peak voltage (0.21 V) for the input concentration of 5 ppb. A linear increase in the peak current of the voltammetric signal was observed with varying ICP factors of time and voltage. Similar phenomenon was observed for 10 and 25 ppb solutions as given in SI Figure S5. This confirms the usefulness of the approach for quantitative analysis.

The efficiency of the device in sensing other metal ions was also studied. For this, 10 ppb of Fe^{2+} , Mn^{2+} , Cu^{2+} and Pb^{2+} were added

separately to 0.1 M H_2SO_4 and subjected to ICP at 30 V for 60 and 150 s and LSV studies were performed. Fig. 4a depicts the voltammetric peak of Fe^{2+} at 0.44 V. The current intensity was 20 μA after concentration for 150 s which was very high as compared to the other ions. The voltammetric peak for oxidation of Cu^{2+} was seen at 0.49 V with an intensity of 2 μA , as shown in Fig. 4b. Fig. 4c represents the LSV of Mn^{2+} . ICP performed at 30 V for 60 and 150 s both showed a peak at 0.1 V during LSV which corresponds to the oxidation of Mn^{2+} on the electrode, while another peak was noted at 0.26 V only in case of 150 s. We speculate that increase in ICP duration increases the local concentration of Mn^{2+} leading to the formation of MnO_2 on the gold electrodes during oxidation following either ECE or disproportionation mechanism [34]. This results in the formation of anisotropic structures on the working electrode and the peak at 0.26 V. The peak at 0.26 V can be attributed to Mn^{4+} which forms during the oxidation of Mn^{2+} following the disproportionation mechanism. The structures deposited on gold working electrodes are shown in SI Figure S6. The LSV of Pb^{2+} is shown in Fig. 4d. The ion Pb^{2+} showed an oxidation peak at 0.16 V with an intensity of 0.05 μA which was the least in the cations analysed. The obtained peak positions were confirmed from literature [35,36], to correspond to the respective ions. It was seen that the concentration of these ions were much higher than As^{3+} .

This can be attributed to the charge of ions in the electrolyte. At acidic pH, arsenic exists as a neutral species while the other ions measured stay as cations. ICP as an electrokinetic technique is highly influenced by ionic size and charge. Cations with larger charge to size ratios tend to migrate faster than those with smaller ratios, which was seen by the reduced concentration of Pb^{2+} as compared to the other cations. The ionic radius of Pb^{2+} is 119 pm, larger compared to Fe^{2+} (77 pm), Cu^{2+} (73 pm) and Mn^{2+} (80 pm). The mobility of cations during ICP is much higher compared to that of anions and neutral species and was attributed to a combination of electrophoretic and electroosmotic phenomena. Arsenic being a neutral species, does not exhibit any electrophoretic mobility and hence the concentration of arsenic by ICP was expected to be caused by only electroosmotic mobility [37,38].

To analyse the capability of our device for field applications, 5 ppb of arsenic was spiked in tap water and tested. Fig. 5a shows the LSV of tap water after ICP. ICP was performed by applying 30 V for 60 s, 150 s and 300 s. It was seen that there were no peaks present in the region of interest which depicted the absence of certain ions. In case of synthetic water sample as given in Fig. 5b, a peak was noted at 0.1 V which increased with increase in the duration for which ICP was performed. The shift in the peak position was due to the change in pH of the electrolyte. Subsequent measurements of tap water and synthetic sample by ICP-MS also showed the same results. The ability of the device to perform in field water was confirmed by analysing water sample from arsenic affected region of West Bengal (India) given in Fig. 5c. The sensor depicted a peak at 0.1 V which can be attributed to arsenic at neutral pH [39,40]. ICP-MS analysis of the field sample showed the arsenic

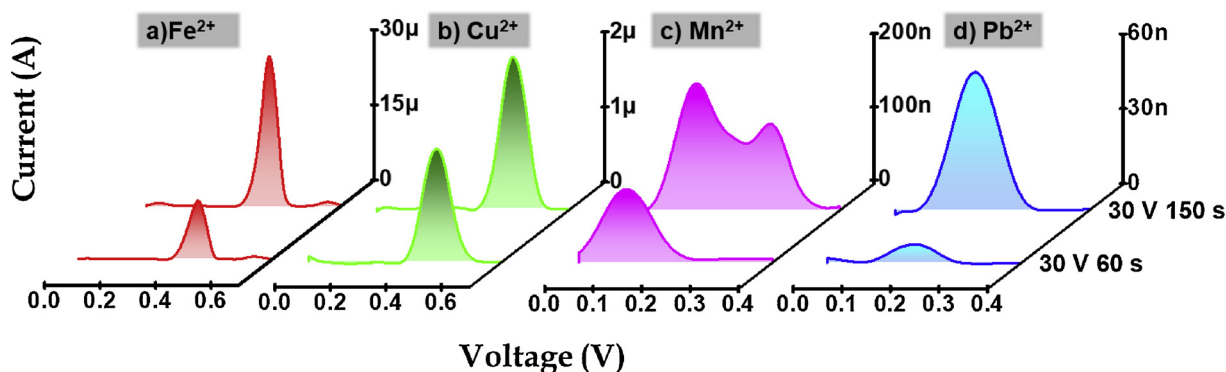


Fig. 4. Electrochemical characterization of 10 ppb of heavy metal ions concentrated at 30 V for 60 and 150 s: a) Fe^{2+} , b) Cu^{2+} , c) Mn^{2+} and d) Pb^{2+} .

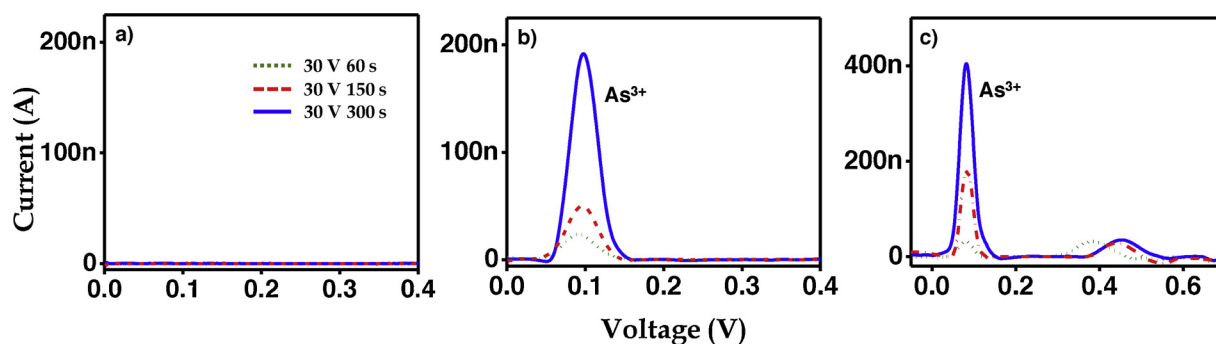


Fig. 5. Electrochemical characterization of a) tap water, b) tap water + 5 ppb As^{3+} and c) field water concentrated at 30 V for 60, 150 and 300 s.

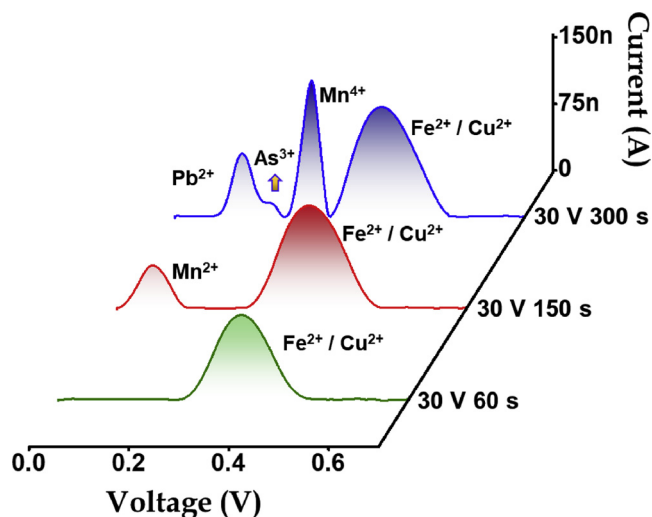


Fig. 6. Electrochemical characterization of 5 ppb of Pb^{2+} , As^{3+} , Fe^{2+} , Mn^{2+} and Cu^{2+} in 0.1 M H_2SO_4 , concentrated at 30 V for 60, 150 and 300 s.

concentration to be about 7 ppb which related to the data previously obtained. Another peak was obtained varying between 0.3 – 0.5 V which was noted to be from Fe^{2+} . The working electrode of our sensor was plain gold electrode with no functionalisation to induce specificity. Fig. 6 shows the performance of our sensor when subjected to multiple ions.

Experiment was conducted on a synthetic multi ion solution created by spiking 5 ppb of Pb^{2+} , As^{3+} , Fe^{2+} , Mn^{2+} and Cu^{2+} in 0.1 M H_2SO_4 . Fig. 6 LSV showed the generation of more peaks as the duration of ICP was increased. When 30 V was applied for 60 s (green trace), a single peak was seen at 0.4 V which was expected to be of Fe^{2+} or Cu^{2+} or a combination of both as both Fe^{2+} and Cu^{2+} were expected to give

peaks in that range. When continued for another 90 s (red trace), another peak at 0.1 V attributed to Mn^{2+} was noted along with the previously observed peak. Increasing the duration to 300 s gave multiple peaks at 0.15, 0.19, 0.26 and 0.45 V which were assigned to Pb^{2+} , As^{3+} , Mn^{4+} and $\text{Fe}^{2+}/\text{Cu}^{2+}$, respectively based on the results obtained previously. During sensing, it was noted that the ions didn't exhibit similar peak intensity during voltammetry even though the initial concentrations of the ions in the electrolyte were maintained the same. The concentration of the ions was seen to follow the conventions of electrophoretic and electroosmotic mobility. The ion, As^{3+} which happens to be neutral at pH 2 exhibits the minimum concentration while the other cations exhibit varying concentrations depending on their ionic radii. This data showed the sensors ability to be used in samples with a combination of ions. To develop a highly specific sensor, the working electrode can be functionalised.

A point of use sensor places high importance on sensitivity and reproducibility. The sensitivity of the sensor for As^{3+} was tested by analysing 1 ppb of As^{3+} in 0.1 M H_2SO_4 as represented in Fig. 7a. Oxidation peak of As^{3+} was obtained at 0.23 V with intensity current of 0.05 μA demonstrating good sensitivity. The time taken for sensing 1 ppb of As^{3+} was noted to be 600 s with no current being observed at lesser time durations. This reemphasises the conjecture that as the duration for ICP was increased, the number of ions concentrated will increase if there is a continuous flow from the inlet. Continuous injection of the sample in the device along with an increased duration for ICP would probably allow us to extend the LOD further.

The reproducibility of the device was confirmed by utilising three different devices and studying their performance under the same applied conditions of 25 ppb of As^{3+} in 0.1 M H_2SO_4 , concentrated at 30 V for 300 s. The devices exhibited very high repeatability with oxidation peak at 0.23 V and a slight variation in current intensity ranging from 2.32 to 2.39 μA as shown in Fig. 7b. The reproducibility of the data was within $\sim \pm 0.08 \mu\text{A}$. The present technique was also compared to other recently reported studies as given in SI Table 2.

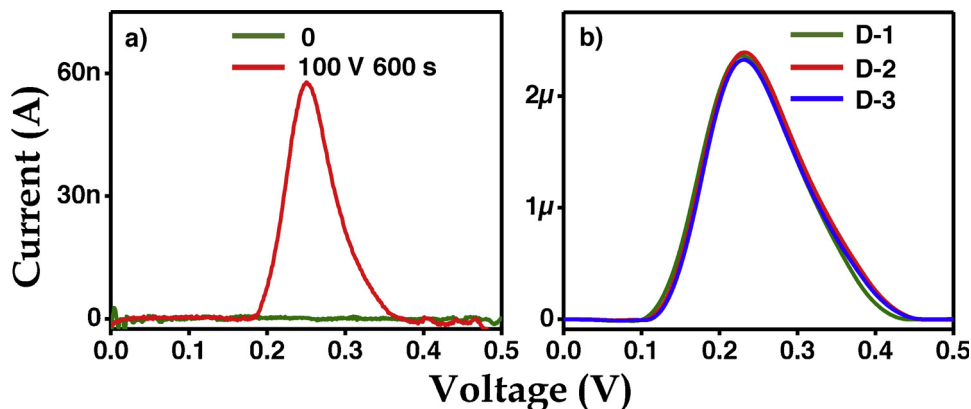


Fig. 7. Electrochemical characterization of a) 1 ppb As^{3+} in 0.1 M H_2SO_4 b) 25 ppb As^{3+} in 0.1 M H_2SO_4 concentrated at 30 V for 300 s for three devices.

The fabricated sensor was single use and non-specific in nature owing to the working electrode being only gold. Specificity in a sensor refers to being completely specific to one analyte in its ideal form. Non-specificity in a sensor leads to decrease in the detection sensitivity of the target as there are at times high similarity between analytes [41]. Also, other ions will interact with the surface of the working electrode, reducing the number of sites for the target to react on. Thus, non-specificity of our device presents a serious limitation for it to be applied in the field conditions. This issue can be rectified by the surface functionalisation of the working electrode with materials exhibiting specificity to arsenic such as nanoparticles [42], MnO₂ [43], enzymes [44], amino acids [45], etc.

4. Conclusion

In this research, we have developed an electrochemical microfluidic sensor with radial microchannels for sensing of arsenite in field water samples. Nanoelectrokinetic pre-concentration by ICP was combined with an electrochemical microfluidic sensor to enable the pre-concentration and detection of the analyte to attain high sensitivity with limited volume of the sample, down to 40 μ L. The sensor fabrication was simplified without the use of valves to ensure portability. The sensor showed the capability to detect As³⁺ down to 1 ppb. The sensor was also tested for the detection of other metal ions such as Cu²⁺, Fe²⁺, Mn²⁺ and Pb²⁺. LSV based response of a mixture of the above mentioned ions was also investigated. The voltammogram showed the presence of peaks specific to each ion of the mixture. The performance of the sensor was stable and repeatable. Surface functionalisation of the working electrode of these sensors can make them extremely analyte specific. The device showed promising capability to be developed as a point of use sensor for resource-limited areas by combining it with a portable electrochemical analyser.

Declaration of Competing Interest

There are no conflicts of interest to declare.

Acknowledgements

We are thankful to the Department of Science and Technology, India, for constantly supporting our research on nanomaterials. The authors are thankful to the Centre for NEMS and Nanophotonics (CNNP), IIT Madras, India for facilitating device fabrication. V.S. is thankful to IIT Madras, India for student fellowship. SJ Kim acknowledged the financial supports from BK21 Plus program of the Creative Engineer Development IT, Seoul National University.

Appendix A. Supplementary data

Supplementary material related to this article can be found, in the online version, at doi:<https://doi.org/10.1016/j.snb.2019.127340>.

References

- [1] Y.-S. Hong, K.-H. Song, J.-Y. Chung, Health effects of chronic arsenic exposure, *J. Prev. Med. Public Health* 47 (2014) 245–252.
- [2] J.H.T. Luong, E. Lam, K.B. Male, Recent advances in electrochemical detection of arsenic in drinking and ground waters, *Anal. Methods* 6 (2014) 6157–6169.
- [3] D.Q. Hung, O. Nekrassova, R.G. Compton, Analytical methods for inorganic arsenic in water: a review, *Talanta* (2004) 269–277.
- [4] J.R. Behari, R. Prakash, Determination of total arsenic content in water by atomic absorption spectroscopy (AAS) using vapour generation assembly (VGA), *Chemosphere* 63 (2006) 17–21.
- [5] I. Komorowicz, D. Baralkiewicz, Determination of total arsenic and arsenic species in drinking water, surface water, wastewater, and snow from Wielkopolska, Kujawy-Pomerania, and Lower Silesia provinces, Poland, *Environ. Monit. Assess.* 188 (2016) 504.
- [6] D.G. Rackus, M.H. Shamsi, A.R. Wheeler, Electrochemistry, biosensors and microfluidics: a convergence of fields, *Chem. Soc. Rev.* 44 (2015) 5320–5340.

- [7] A. Ainla, M.P.S. Mousavi, M.-N. Tsaloglou, J. Redston, J.G. Bell, M.T. Fernández-Abedul, et al., Open-source potentiostat for wireless electrochemical detection with smartphones, *Anal. Chem.* 90 (2018) 6240–6246.
- [8] A. Nemiroski, D.C. Christodouleas, J.W. Hennek, A.A. Kumar, E.J. Maxwell, M.T. Fernández-Abedul, et al., Universal mobile electrochemical detector designed for use in resource-limited applications, *Proc. Natl. Acad. Sci. U. S. A.* 111 (2014) 11984.
- [9] A.C. Sun, C. Yao, A.G. Venkatesh, D.A. Hall, An efficient power harvesting mobile phone-based electrochemical biosensor for point-of-care health monitoring, *Sens. Actuators B, Chem.* 235 (2016) 126–135.
- [10] S. Li, C. Zhang, S. Wang, Q. Liu, H. Feng, X. Ma, et al., Electrochemical microfluidics techniques for heavy metal ion detection, *Analyst* 143 (2018) 4230–4246.
- [11] D.R. Reyes, D. Iossifidis, P.-A. Auroux, A. Manz, Micro total analysis systems. 1. Introduction, theory, and technology, *Anal. Chem.* 74 (2002) 2623–2636.
- [12] C.T. Culbertson, T.G. Mickleburgh, S.A. Stewart-James, K.A. Sellens, M. Pressnall, Micro total analysis systems: fundamental advances and biological applications, *Anal. Chem.* 86 (2014) 95–118.
- [13] W.-L. Hsu, D.W. Inglis, M.A. Startsev, E.M. Goldys, M.R. Davidson, D.J.E. Harvie, Isoelectric focusing in a silica nanofluidic channel: effects of electromigration and electroosmosis, *Anal. Chem.* 86 (2014) 8711–8718.
- [14] M. Solsona, E.Y. Westerbeek, J.G. Bomer, W. Olthuis, A. van den Berg, Gradient in the electric field for particle position detection in microfluidic channels, *Lab Chip* 19 (2019) 1054–1059.
- [15] J. Dai, T. Ito, L. Sun, R.M. Crooks, Electrokinetic trapping and concentration enrichment of DNA in a microfluidic channel, *J. Am. Chem. Soc.* 125 (2003) 13026–13027.
- [16] T. Salafi, K.K. Zeming, Y. Zhang, Advancements in microfluidics for nanoparticle separation, *Lab Chip* 17 (2017) 11–33.
- [17] C. Zhao, Z. Ge, C. Yang, Microfluidic techniques for analytes concentration, *Micromachines* 8 (2017) 28.
- [18] Y. Kang, D. Li, Electrokinetic motion of particles and cells in microchannels, *Microfluid. Nanofluidics* 6 (2009) 431–460.
- [19] Q. Pu, J. Yun, H. Temkin, S. Liu, Ion-enrichment and ion-depletion effect of nanochannel structures, *Nano Lett.* 4 (2004) 1099–1103.
- [20] Z. Slouka, S. Senapati, H.-C. Chang, Microfluidic systems with ion-selective membranes, *Annu. Rev. Anal. Chem.* 7 (2014) 317–335.
- [21] S.J. Kim, Y.-A. Song, J. Han, Nanofluidic concentration devices for biomolecules utilizing ion concentration polarization: theory, fabrication, and applications, *Chem. Soc. Rev.* 39 (2010) 912–922.
- [22] S.Y. Son, S. Lee, H. Lee, S.J. Kim, Engineered nanofluidic pre-concentration devices by ion concentration polarization, *Biochip J.* 10 (2016) 251–261.
- [23] H. Lee, J. Choi, E. Jeong, S. Baek, H.C. Kim, J.-H. Chae, et al., dCas9-mediated nanoelectrokinetic direct detection of target gene for liquid biopsy, *Nano Lett.* 18 (2018) 7642–7650.
- [24] W. Ouyang, X. Ye, Z. Li, J. Han, Deciphering ion concentration polarization-based electrokinetic molecular concentration at the micro-nanofluidic interface: theoretical limits and scaling laws, *Nanoscale* 10 (2018) 15187–15194.
- [25] M. Kim, M. Jia, T. Kim, Ion concentration polarization in a single and open microchannel induced by a surface-patterned perm-selective film, *Analyst* 138 (2013) 1370–1378.
- [26] Y. Xia, G.M. Whitesides, Soft lithography, *Ann. Rev. Mater. Sci.* 28 (1998) 153–184.
- [27] S. Lee, S. Park, N.L. Jeon, S.J. Kim, Nanoelectrokinetic radial preconcentrator/extractor based on ion concentration polarization, 2017 IEEE 30th International Conference on Micro Electro Mechanical Systems (MEMS), IEEE (2017) 1285–1288.
- [28] S. Lee, S. Park, W. Kim, S. Moon, H.-Y. Kim, H. Lee, et al., Nanoelectrokinetic bufferchannel-less radial preconcentrator and online extractor by tunable ion depletion layer, *Biomicrofluidics* 13 (2019) 034113.
- [29] C.L. Druzgalski, M.B. Andersen, A. Mani, Direct numerical simulation of electroconvective instability and hydrodynamic chaos near an ion-selective surface, *Phys. Fluids* 25 (2013) 110804.
- [30] S.A. Hong, Y.-J. Kim, S.J. Kim, S. Yang, Electrochemical detection of methylated DNA on a microfluidic chip with nanoelectrokinetic pre-concentration, *Biosens. Bioelectron.* 107 (2018) 103–110.
- [31] W.R. Cullen, K.J. Reimer, Arsenic speciation in the environment, *Chem. Rev.* 89 (1989) 713–764.
- [32] M.E. Hyde, C.E. Banks, R.G. Compton, Anodic stripping voltammetry: an AFM study of some problems and limitations, *Electroanalysis* 16 (2004) 345–354.
- [33] H. Jeon, H. Lee, K.H. Kang, G. Lim, Ion concentration polarization-based continuous separation device using electrical repulsion in the depletion region, *Sci. Rep.* 3 (2013) 3483.
- [34] A. Manivel, N. Ilayaraja, D. Velayutham, M. Noel, Medium effects on the electro-deposition of MnO₂ on glassy carbon electrode: a comparative study in alkane, perfluoro alkane carboxylic acids and methanesulphonic acid, *Electrochim. Acta* 52 (2007) 7841–7848.
- [35] G.W. Tindall, S. Bruckenstein, A ring-disk electrode study of the electrochemical reduction of copper(II) in 0.2M sulfuric acid on platinum, *Anal. Chem.* 40 (1968) 1051–1054.
- [36] P. Vanýsek, CRC Handbook of Chemistry and Physics, 91 edition, CRC Press, 2010.
- [37] D. Yan, C. Yang, N.-T. Nguyen, X. Huang, Electrokinetic flow in Microchannels with finite reservoir size effects, *J. Phys. Conf. Ser.* 34 (2006) 385–392.
- [38] J.G. Santiago, Electroosmotic flows in Microchannels with finite inertial and pressure forces, *Anal. Chem.* 73 (2001) 2353–2365.
- [39] D. Yamada, T.A. Ivandini, M. Komatsu, A. Fujishima, Y. Einaga, Anodic stripping voltammetry of inorganic species of As³⁺ and As⁵⁺ at gold-modified boron doped diamond electrodes, *J. Electroanal. Chem.* 615 (2008) 145–153.
- [40] A.D. Robles, S.N. Vettorelo, M. Gerpe, F. Garay, The electrochemical reaction

- mechanism of arsenic on gold analyzed by anodic stripping Square-wave voltammetry, *Electrochim. Acta* 227 (2017) 447–454.
- [41] W.J. Peveler, M. Yazdani, V.M. Rotello, Selectivity and specificity: pros and cons in sensing, *ACS Sens.* 1 (2016) 1282–1285.
- [42] N. Moghimi, M. Mohapatra, K.T. Leung, Bimetallic nanoparticles for arsenic detection, *Anal. Chem.* 87 (2015) 5546–5552.
- [43] S. Zhou, X. Han, H. Fan, Y. Liu, Electrochemical sensing toward trace As(III) based on mesoporous MnFe₂O₄/Au hybrid nanospheres modified glass carbon electrode, *Sens. Basel (Basel)* 16 (2016) 935.
- [44] M. Park, S.-L. Tsai, W. Chen, Microbial biosensors: engineered microorganisms as the sensing machinery, *Sens. Basel (Basel)* 13 (2013) 5777–5795.
- [45] T. Yang, X.-X. Zhang, J.-Y. Yang, Y.-T. Wang, M.-L. Chen, Screening arsenic(III)-binding peptide for colorimetric detection of arsenic(III) based on the peptide induced aggregation of gold nanoparticles, *Talanta* 177 (2018) 212–216.